N63-21890

NASA TECHNICAL NOTE

NASA TN D-1879

NASA TN D-1879

THERMIONIC EMISSION FROM CESIUM-COATED ELECTROSTATIC ION-THRUSTER ELECTRODES

by Thaine W. Reynolds and Edward A. Richley;
Lewis Research Center,
Cleveland, Ohio

NATIONAL AERONAUTICS AND SPACE ADMINISTRATION • WASHINGTON, D. C. • SEPTEMBER 1963

TECHNICAL NOTE D-1879

THERMIONIC EMISSION FROM CESIUM-COATED ELECTROSTATIC ION-THRUSTER ELECTRODES

By Thaine W. Reynolds and Edward A. Richley

Lewis Research Center
Cleveland, Ohio

NATIONAL AERONAUTICS AND SPACE ADMINISTRATION

NATIONAL AERONAUTICS AND SPACE ADMINISTRATION

TECHNICAL NOTE D-1879

THERMIONIC EMISSION FROM CESIUM-COATED ELECTROSTATIC ION-THRUSTOR ELECTRODES

By Thaine W. Reynolds and Edward A. Richley

SUMMARY

An analysis was made of the possible thermionic electron-emission currents attainable from cesium-coated tungsten accelerator electrodes in ion thrustors. Both an axisymmetric and a rectangular electrode configuration were examined for accelerator temperatures near the values yielding maximum emission. The electron-emission behavior was substantially the same for both configurations.

An electron-emission current equal to about 4 percent of the ion-beam current is possible for cases where the neutral-cesium flux to the accelerator electrode comes directly from the ionizer. If a background gas pressure of cesium can build up in the interelectrode space, thermionic electron-emission currents as high as 40 percent of the ion-beam current can result. These values of electron current are of sufficient magnitude to obscure measurements of the true ion-impingement currents on the accelerator electrode.

In actual thrustor operation, maintaining the accelerator at a temperature $\pm 100^{\circ}$ K away from that at which peak electron emission occurs could reduce the electron emission current by about an order of magnitude.

INTRODUCTION

The development of ion thrustors for space-flight applications requires the attainment of systems that will operate continuously for long periods of time. To attain a long lifetime for the thrustor, it is necessary to have an accelerator-electrode structure that results in very low ion-impingement currents - of the order of 0.1 percent or less of the normal ion beam currents (refs. 1 to 3). The attainment of such low impingement currents is a major design problem.

In an experiment in which accelerator-electrode drain currents are measured with an ammeter, it is impossible to distinguish between electron current being emitted from and ion current impinging on the accelerator electrode. It is only ion impingement that is responsible for electrode erosion and, hence, shortened electrode life. It is important, therefore, in evaluating thrustor performance from experimental results, to know the magnitude of electron-emission currents so that a determination of the ion-impingement current may be made.

Calculations of thermionic electron emission from cesium-coated tungsten accelerator electrodes are presented for a range of expected neutral-cesium emission fluxes. The qualitative effect of varying the accelerator material is discussed.

METHOD OF ANALYSIS

Models and Assumptions

Two configurations are analyzed: an axisymmetric (cylindrical) beam (fig. 1 and sketch (a)) and a rectangular (slab) beam (fig. 2 and sketch (b)).

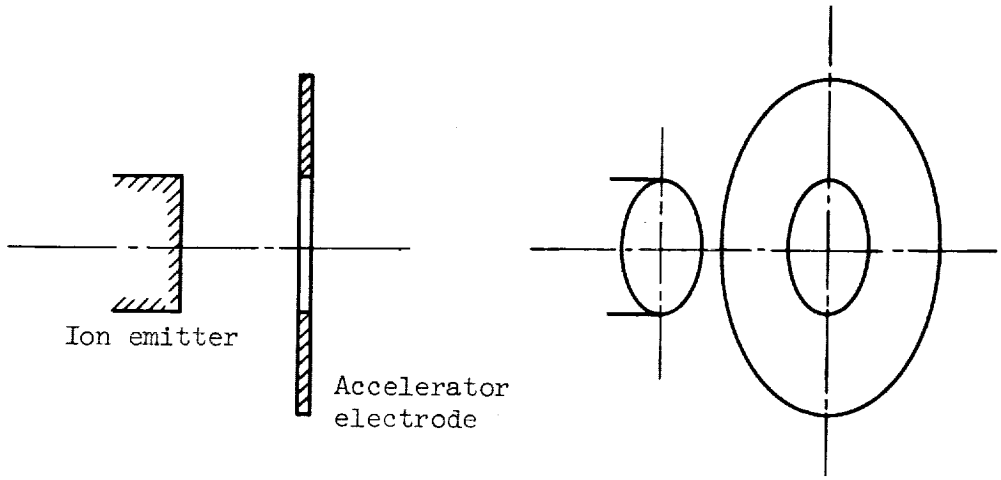

(a)

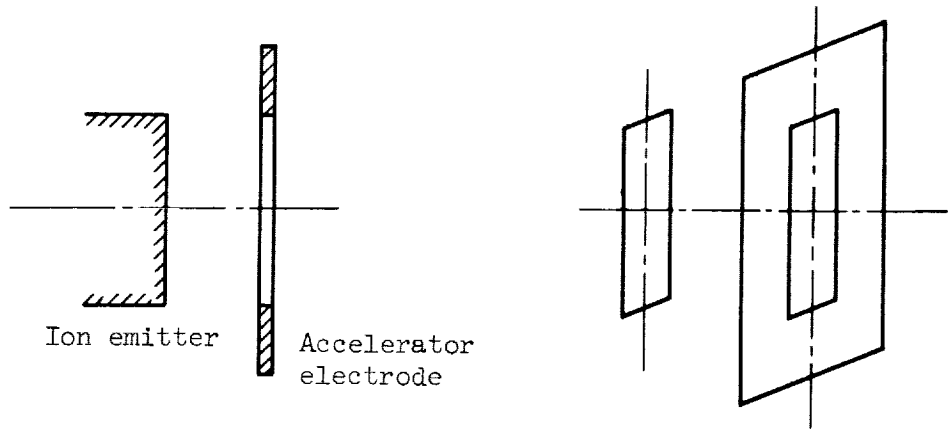

(b)

The following analysis is concerned only with the effects that arise in connection with the nonionized fraction of cesium atoms that leave the emitter (sketch (c)). The fate of the cesium ions formed at the emitter is unimportant

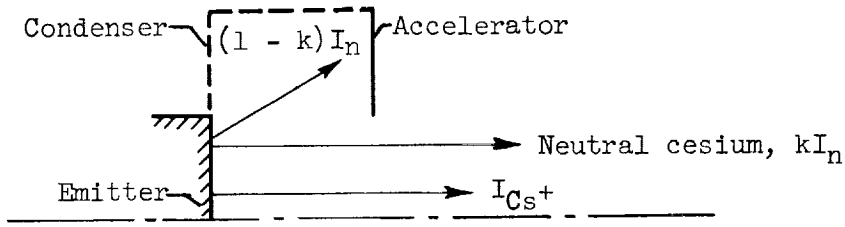

(c)

to the analysis; therefore, all cesium ions I_{Cs^+} can be assumed to pass through the accelerator opening.

The nonionized, or neutral, cesium atoms I_n are assumed to leave the emitter with a diffuse emission pattern. Some of them (the fraction k) go directly through the accelerator opening. The remainder (the fraction 1 - k) are directed into the interelectrode space. It is this fraction of the neutral-cesium efflux from the ion emitter that enters into adsorption equilibrium with the accelerator electrode and gives rise to thermionic electron emission from the upstream face of the accelerator electrode.

As will be shown later, the magnitude of the emitted electron current increases with increasing arrival rate of cesium atoms at the accelerator-electrode surface. For this reason, two cases were developed in the analysis for treating the neutral-cesium fraction 1 - k. These two cases yield lower and upper limits to the arrival rate of neutral cesium at the accelerator and, hence, can be considered as "limiting" cases for the thermionically emitted electron current.

For case 1, the neutral cesium from the emitter that reaches the accelerator electrode directly results in a distribution in the arrival rate with location on the accelerator. In this case, the cesium atoms that do not impinge directly on the accelerator, along with those that are desorbed from the accelerator surface, are assumed to "condense" out of the system.

For case 2, the neutral-atom arrival rate at the upstream face of the accelerator electrode is assumed uniform. This case may arise if, for example, no condensation of cesium atoms occurs in the interelectrode space. A background gas pressure of neutral-cesium atoms is thus built up in this region; consequently, the eventual loss of these atoms from the system is through the exhaust aperture in the accelerator.

Although there are several other processes that could affect the electron emission from the accelerator, these processes are not considered in the present paper.

Calculations of Arrival Rate

Many of the equations developed in this section will be recognized as the Knudsen flow relations of rarefied-gas dynamics or the analogous relations of

radiant heat transfer. Various forms of these relations are common in the literature (refs. 4 to 6). For completeness, the development of the specific forms used in the subsequent analysis is given herein.

Axisymmetric beam. - For the axisymmetric beam arrangement, the pertinent variables are shown in figure 1. Let ν_a be the neutral flux (atoms/(sq cm)(sec)) leaving the emitter. This flux will be assumed uniform over the emitter area. Under the assumption of diffuse emission, the directed flux leaving the unit area dA_1 that arrives at an area on the accelerator dA_2 is

$$d(\mu)_{r_2} = \frac{\nu_a \cos^2\alpha}{\pi l^2} r_1 \, dr_1 \, d\theta_1 \tag{1}$$

where l is the distance from dA_1 to dA_2 and α is the angle between the normal to dA_1 and l. (All symbols are defined in the appendix.) Then,

$$\cos \alpha = \frac{L}{l} \tag{2}$$

and from the law of cosines

$$l^2 = r_1^2 + r_2^2 - 2r_1r_2 \cos(\theta_1 - \theta_2) + L^2 \tag{3}$$

Substituting equations (2) and (3) into (1) and setting up the integral over dA_1 yield

$$\left(\frac{\mu}{\nu_a}\right)_{r_2,\theta_2} = \int_0^R dr_1 \int_0^\pi d\theta_1 \left\{ \frac{2r_1L^2}{\pi\left[r_1^2 + r_2^2 - 2r_1r_2 \cos(\theta_1 - \theta_2) + L^2\right]^2} \right\} \tag{4}$$

In this instance, because of the axial symmetry, θ_2 can be set equal to zero. That is, μ/ν_a is examined along a radius r_2 at $\theta_2 = 0$. Since the result

$$\left(\frac{\mu}{\nu_a}\right)_{r_2} = \frac{2L^2}{\pi} \int_0^R dr_1 \int_0^\pi \frac{r_1 \, d\theta_1}{\left(r_1^2 + r_2^2 - 2r_1r_2 \cos \theta_1 + L^2\right)^2} \tag{5}$$

is independent of θ_2, the solution will be a function of r_2 only.

Integration of equation (5) yields the following relation:

$$\left(\frac{\mu}{\nu_a}\right)_{r_2} = \frac{1}{2}\left\{1 - \frac{\left(\frac{L}{R}\right)^2 - 1 + \left(\frac{r_2}{R}\right)^2}{\sqrt{\left[1 + \left(\frac{L}{R}\right)^2 + \left(\frac{r_2}{R}\right)^2\right]^2 - 4\left(\frac{r_2}{R}\right)^2}}\right\} \tag{6}$$

Equation (6) expresses the arrival rate per unit area of the accelerator in terms of the neutral-emission rate from the ionizer.

When the radius of the accelerator aperture equals the radius of the emitter, the fraction of the emitted neutral particles that go directly through the opening is

$$k = \frac{1}{\pi R^2}\int_0^R \left(\frac{\mu}{\nu_a}\right)_{r_2} 2\pi r_2 \, dr_2 \tag{7}$$

or

$$k = 1 + \frac{1}{2}\left(\frac{L}{R}\right)^2 - \frac{L}{2R}\sqrt{(L/R)^2 + 4} \tag{8}$$

For case 2, wherein it is assumed that the fraction $1 - k$ builds up a background pressure in the interelectrode space before it eventually escapes out the accelerator opening, the effective arrival rate of this background gas anywhere in the interelectrode space is assumed uniform and can be determined by the requirement

$$\mu A_{ao} = (1 - k)\nu_a A_e \tag{9}$$

When the area of the accelerator opening is equal to the emitter area,

$$\frac{\mu}{\nu_a} = 1 - k \tag{10}$$

Equation (10) is general in the sense that it is independent of the geometry of a given configuration.

Values of the arrival-rate ratio μ/ν_a from relations (6) and (10) will be used to estimate the lower and the upper limits of electron-emission currents, respectively, from the upstream surface of the accelerator in the axisymmetric configurations.

Rectangular beam. - The pertinent variables used for the rectangular beam are shown in figure 2. Again, ν_a is the neutral-cesium flux from the emitter. For case 1, the particle arrival rate at the accelerator is given by the relation

$$d(\mu) = \frac{\nu_a \cos^2\alpha}{\pi l^2}\, dx\, dy \tag{11}$$

where

$$l^2 = L^2 + (v - y)^2 + (u - x)^2 \tag{12}$$

and

$$\cos\alpha = \frac{L}{l} \tag{13}$$

Substituting equations (12) and (13) into (11) and setting up the integral over the emitter area yield

$$\left(\frac{\mu}{\nu_a}\right)_{u,v} = \frac{L^2}{\pi}\int_{-W/2}^{+W/2} dx \int_{-Y/2}^{+Y/2} dy\, \frac{1}{\left[L^2 + (v - y)^2 + (u - x)^2\right]^2} \tag{14}$$

Integration of equation (14) yields the following relation:

$$\begin{aligned}\left(\frac{\mu}{\nu_a}\right)_{u,v} = \frac{1}{2\pi}\Bigg\{ & \frac{\frac{Y}{2} - v}{\sqrt{L^2 + \left(\frac{Y}{2} - v\right)^2}}\left[\tan^{-1}\frac{\frac{W}{2} + u}{\sqrt{L^2 + \left(\frac{Y}{2} - v\right)^2}} + \tan^{-1}\frac{\frac{W}{2} - u}{\sqrt{L^2 + \left(\frac{Y}{2} - v\right)^2}}\right] \\ & + \frac{\frac{Y}{2} + v}{\sqrt{L^2 + \left(\frac{Y}{2} + v\right)^2}}\left[\tan^{-1}\frac{\frac{W}{2} + u}{\sqrt{L^2 + \left(\frac{Y}{2} + v\right)^2}} + \tan^{-1}\frac{\frac{W}{2} - u}{\sqrt{L^2 + \left(\frac{Y}{2} + v\right)^2}}\right] \\ & + \frac{\frac{W}{2} - u}{\sqrt{L^2 + \left(\frac{W}{2} - u\right)^2}}\left[\tan^{-1}\frac{\frac{Y}{2} + v}{\sqrt{L^2 + \left(\frac{W}{2} - u\right)^2}} + \tan^{-1}\frac{\frac{Y}{2} - v}{\sqrt{L^2 + \left(\frac{W}{2} - u\right)^2}}\right] \\ & + \frac{\frac{W}{2} + u}{\sqrt{L^2 + \left(\frac{W}{2} + u\right)^2}}\left[\tan^{-1}\frac{\frac{Y}{2} + v}{\sqrt{L^2 + \left(\frac{W}{2} + u\right)^2}} + \tan^{-1}\frac{\frac{Y}{2} - v}{\sqrt{L^2 + \left(\frac{W}{2} + u\right)^2}}\right]\Bigg\}\end{aligned} \tag{15}$$

Equation (15) gives the arrival rate per unit area at the accelerator plane for the rectangular configuration when the principal values for the arc tangent ($-\pi/2$ to $+\pi/2$) are used. A special configuration of the rectangular geometry

is the one in which the ratio of emitter length to width Y/W becomes large. The limiting value of equation (15) when Y/W approaches infinity is

$$\left(\frac{\mu}{\nu_a}\right)_{u,Y=\infty} = \frac{1}{2}\left[\frac{1 - \frac{2u}{W}}{\sqrt{4\left(\frac{L}{W}\right)^2 + \left(1 - \frac{2u}{W}\right)^2}} + \frac{1 + \frac{2u}{W}}{\sqrt{4\left(\frac{L}{W}\right)^2 + \left(1 + \frac{2u}{W}\right)^2}}\right] \tag{16}$$

When the width of the accelerator opening equals the width of the emitter and $Y/W = \infty$, the value of k, the fraction of emitted neutrals that go directly out the accelerator opening, is given by

$$k = \sqrt{1 + \left(\frac{L}{W}\right)^2} - \frac{L}{W} \tag{17}$$

For the uniform-arrival-rate assumption (case 2), the value of μ/ν_a is obtained, as for the axisymmetric beam, by means of equation (10).

Calculation of Electron Emission

The neutral-cesium arrival rate on the surface of the accelerator (possibly made of some refractory metal such as tungsten, molybdenum, or tantalum), at a given accelerator temperature results in a variation in concentration of adsorbed cesium over the accelerator. This adsorbed layer lowers the work function of the electrode material and results in electron emission.

The magnitude of electron-emission current for cesium-coated surfaces is usually presented in the form of S-shaped curves such as those shown in figure 3(a) for cesium on tungsten. An interpretation of the physical behavior of the adsorbed cesium layer on the tungsten surface as the temperature of the surface is varied may aid in understanding the analysis that follows. A curve for one particular arrival rate of cesium is illustrated in sketch (d). At a high

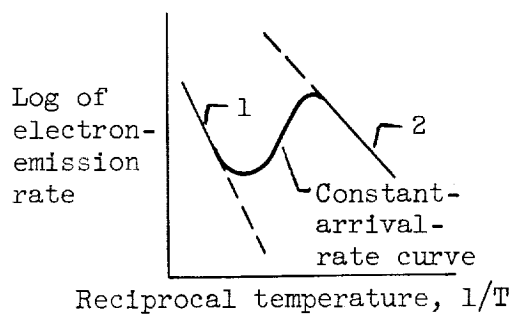

(d)

temperature (to the left in sketch (d)), there is little or no cesium adsorbed on the tungsten. The electron-emission rate for this condition (i.e., for clean tungsten) is given by line 1, which is the well-known Richardson-Dushman equation for thermionic emission. As the tungsten temperature is decreased (to the

right in sketch (d)), an adsorbed layer of cesium forms on the surface. This layer lowers the work function and tends to increase the electron-emission rate. At the same time, the lower temperature tends to decrease the emission rate. The resulting electron emission is given by the solid line. In the middle region of the S-curve, the decrease in the work function more than compensates for the lowering of the temperature. Consequently, the electron-emission rate increases and reaches a maximum. Beyond this point, increased adsorption does not affect the work function sufficiently to overcome the lowering of the temperature; thus, the electron-emission (given by line 2) decreases.

Not considered in this report is the effect of an electric field at the surface (the Schottky effect, ref. 7). For the magnitude of electric fields usually encountered in experimental thrustors, this effect could approximately double the values to be cited.

For the purposes of this report, the electron-emission-rate data of figure 3(a) were replotted in the forms shown in figures 3(b) and (c) for tungsten and molybdenum, respectively. These are plots of electron emission against cesium-atom arrival rate for lines of constant temperature of the base metal. Figure 4 shows the temperature at which peak electron emission occurs for a given arrival rate of cesium on tungsten or molybdenum. The data used for the cesium-tungsten system were taken from reference 7, and for the cesium-molybdenum system from reference 8.

Once the cesium flux at a point on the accelerator electrode has been determined, the electron-emission rate is obtained from figure 3. Values are assumed for ν_a and the accelerator-electrode temperature. For a given point on the accelerator of the configuration being considered, the value of μ/ν_a is determined from the appropriate equation (i.e., eq. (6), (10), (15), or (16)). This value of μ/ν_a multiplied by the assumed ν_a gives the "local" value of μ. With this value of μ and the assumed accelerator-electrode temperature, the "local" electron-emission rate is obtained from figure 3. By this procedure, the electron-emission rate distribution over the upstream surface of the accelerator-electrode surface can be determined. The total electron emission from the electrode is then obtained by integrating the local emission rates over the area involved.

The parameter of particular interest in this study is the ratio of total electron-emission current to total ion-beam current I_e/I_{Cs^+}. To obtain this ratio, the integrated electron-emission rates are divided by the total ion-beam current. By defining f as the ratio of neutral-atom- to ion-emission rate from the ion emitter, that is

$$f = \frac{\nu_a}{\nu_{Cs^+}} \tag{18}$$

the expressions for the ratio of I_e/I_{Cs^+} can be written as follows:

For the axisymmetric beam with distributed arrival rate:

$$\frac{I_e}{I_{Cs^+}} = \frac{f}{\nu_a \pi R^2} \int_R^{nR} (\nu_e)_r 2\pi r \, dr = 2f \int_1^n \left(\frac{\nu_e}{\nu_a}\right)\left(\frac{r}{R}\right) d\left(\frac{r}{R}\right) \tag{19}$$

where n is the ratio of the accelerator outer to inner radius.

For the axisymmetric beam with uniform arrival rate:

$$\frac{I_e}{I_{Cs^+}} = \frac{\nu_e}{\nu_a} (n^2 - 1) f \tag{20}$$

For the rectangular beam with distributed arrival rate:

$$\frac{I_e}{I_{Cs^+}} = \frac{4f}{YW}\left[\int_0^{U/2} du \int_0^{V/2} dv \left(\frac{\nu_e}{\nu_a}\right)_{u,v} - \int_0^{W/2} du \int_0^{Y/2} dv \left(\frac{\nu_e}{\nu_a}\right)_{u,v}\right] \tag{21}$$

For the rectangular beam with uniform arrival rate:

$$\frac{I_e}{I_{Cs^+}} = \frac{\nu_e}{\nu_a}\left(\frac{UV}{YW} - 1\right) f = \frac{\nu_e}{\nu_a}\left(n \frac{V}{Y} - 1\right) f \tag{22}$$

where n is the ratio of accelerator to emitter width. When $Y = V$, which includes $Y/W = \infty$, equation (22) becomes

$$\frac{I_e}{I_{Cs^+}} = \frac{\nu_e}{\nu_a}\left(\frac{U}{W} - 1\right) f = \frac{\nu_e}{\nu_a} (n - 1) f \tag{23}$$

RESULTS AND DISCUSSION

Arrival Rates and Electron-Emission Rates

Axisymmetric beam. - Values of μ/ν_a, the ratio of the arrival rate of neutral atoms at the accelerator to the emission rate of neutral atoms from the emitter, were calculated for case 1. Distribution curves for several values of the nondimensional accelerator spacing ratio L/R are shown in figure 5. Also shown in figure 5 are values of k from equation (8).

From the distribution curve for the configuration in which $L/R = 2$ and the electron-emission-rate curves for the cesium-tungsten system (fig. 3(b)),

the electron-emission-rate distribution from the accelerator was determined for several assumed accelerator temperatures and neutral-atom emission rates.

The neutral-atom emission rate ν_a can be written in terms of the ion-current density j and the neutral-atom to ion-emission fraction f as

$$\nu_a = 6.25\times10^{14} fj \qquad \frac{\text{atoms}}{(\text{sq cm})(\text{sec})} \tag{24}$$

where j is in amperes per square meter. Values of ν_a of 10^{14} to 10^{16} were assumed. These rates correspond to 0.16 to 16 percent of an ion-beam-current density of 100 amperes per square meter and are typical of observed values (ref. 9).

Typical electron-emission distributions resulting from these calculations are shown in figure 6. The electron distribution curves do not always have the same shape as the atom-arrival-rate curves, because the emission rate is not linearly related to the arrival rate.

As shown in figure 3(a), a maximum electron emission occurs for a given arrival rate of cesium at some particular surface temperature. For the arrival rates of neutral particles encountered herein, the temperature for maximum emission is in the range from 600° to 1000° K, and the calculations cover this range.

The total electron-emission currents were obtained by integrating curves of the type in figure 6 over the electrode area. The results for the axisymmetric beam are plotted in figure 7. The function $(1/f)(I_e/I_{Cs^+})$, which is equal to ν_e/ν_a, is plotted against temperature. The integrations of figure 6 were carried out for assumed accelerator outer radii equal to 2R and 3R, that is, for $n = 2$ and 3, respectively.

A corresponding parameter ν_e/ν_a was calculated by means of equation (10) for case 2 (uniform arrival rate). This parameter is plotted against temperature in figure 8.

Rectangular beam. - The variation in the u-direction of the arrival-rate ratio μ/ν_a for the rectangular configuration with $Y/W = \infty$ is shown in figure 9 for several values of L/W. The variation in the u- and v-directions of the ratio μ/ν_a for a finite-length configuration ($Y/W = 10$) were calculated from equation (16) and are shown in figure 10. Compare the $L/W = 1$ curve of figure 9 with the curves of figure 10, which are also for $L/W = 1$. The curve for $v/Y = 0$ (fig. 10(a)) is identical with the $L/W = 1$ curve of figure 9. At $v/Y = 0.4$, the curve of figure 10(a) is only slightly lower than the $v/Y = 0$ curve. Thus, the distribution in the u-direction for a finite-length configuration, where the length-to-width ratio is 10, is substantially the same as that of the infinite-length configuration. From examining figure 10(b), it can be seen that the distribution is relatively flat over about 80 percent of the length. From these considerations, it appears that calculations based on the infinite-length rectangular configuration will yield results typical of the finite-length configuration so long as the length-to-width ratio of the emitter

is greater than about 10.

The remaining calculations for the rectangular configuration were carried out for $Y/W = \infty$ by using the arrival-rate ratio μ/ν_a given by equation (16).

From the arrival-rate distribution curve of figure 9 for $L/W = 1$ and electron emission from the cesium-tungsten system (fig. 3(b)), the electron-emission distribution rates for several assumed accelerator temperatures were calculated. Typical curves are shown in figure 11. The essential features of the distribution are the same as for the axisymmetric beam, with the exception that the electron emission does not, in general, drop off as rapidly with distance from the centerline for the rectangular beam because the neutral flux falls off less rapidly.

Electron-emission-rate distribution curves similar to those of figure 11 were integrated over accelerator-electrode widths of two and three times the emitter width (i.e., $U/W = 2$ and 3, respectively). The results are shown in figure 12, where the function $(1/f)(I_e/I_{Cs^+})$ is plotted against the accelerator temperature.

The arrival-rate ratio μ/ν_a for the uniform-arrival-rate case is obtained by using the same relation as for the axisymmetric beam (eq. (10)). Thus, the electron emission for the rectangular beam may be obtained from the curves of figure 8 by using the appropriate value of k from equation (17).

Electron-Ion Current Ratios

Since the purpose of this analysis was to arrive at a comparison of the possible electron-emission currents from a coated accelerator electrode with the attendant total ion current, some of these current ratios will now be determined from the curves just presented.

The actual magnitude of electron current varies strongly with metal temperature, as is noted in the curves of figures 7, 8, and 12. Since accelerator temperatures for actual thrustors can fall within the range of temperatures cited (ref. 10), it is of interest to estimate the peak electron currents obtainable in each case considered. The calculation of electron-emission currents was carried out for a value of accelerator spacing L equal to the full width of the emitter, that is, for $L/R = 2$ for the axisymmetric beam, and for $L/W = 1$ for the rectangular beam. It may be seen from the arrival-rate-distribution curves of figures 5 and 9 that the results for other spacing ratios of practical interest would be little different from those calculated for the present configurations.

For distributed neutral-cesium arrival rates, the total electron-emission currents are given by the curves of figures 7 and 12. The peak values of $(1/f)(I_e/I_{Cs^+})$ in these figures vary from about 0.18 to 0.24 ($n = 2$) and from 0.29 to 0.42 ($n = 3$) for the axisymmetric configuration, and from 0.13 to 0.14 ($n = 2$) and from 0.19 to 0.22 ($n = 3$) for the rectangular configuration. These peak values were relatively independent of neutral-atom arrival rate. The tem-

perature at which the peak emission occurred increased as the atom arrival rate increased.

The ratio of electron current to ion current actually depends on the neutral fraction f. This fraction may vary in particular instances from about 0.01 to 0.10 (ref. 9) for ion-current densities up to approximately 200 amperes per square meter. With this range of variation in f considered in conjunction with the values cited in the previous paragraph, it may be estimated that electron-emission currents can range from about 0.0013 to 0.0420 times the ion-beam current. Electron-emission currents of this magnitude can completely obscure the true ion-impingement currents as determined from conventional meter readings.

For the case wherein a uniform arrival rate at the accelerator electrode was assumed, the peak electron emissions may be determined from figure 8. This figure is applicable to either the axisymmetric- or rectangular-beam configuration. The peak value of $(1/f)(\nu_e/\nu_{Cs^+})$ depends on the value of k, which is a function of the L/R or L/W of the configuration. For an axisymmetric configuration with $L/R = 2$, $k = 0.17$ and the peak value of $(1/f)(\nu_e/\nu_{Cs^+})$ is about 0.5. For a rectangular configuration with $L/W = 1.0$, $k = 0.414$ and the peak value of $(1/f)(\nu_e\nu_{Cs^+})$ is about 0.3.

Values of I_e/I_{Cs^+} for these conditions, then, depend not only on the neutral fraction f, but also on the size of the accelerator electrode n (eqs. (20) and (23)). For the axisymmetric configuration, equation (20) reduces to

$$\begin{aligned}\frac{I_e}{I_{Cs^+}} &= 0.5(n^2 - 1)f \\ &= 1.5\ f \quad \text{for} \quad n = 2 \\ &= 4\ f \quad \text{for} \quad n = 3\end{aligned} \tag{25}$$

Again, for values of f ranging from 0.01 to 0.10, possible values of I_e/I_{Cs^+} are 0.015 to 0.150 for $n = 2$ and 0.04 to 0.40 for $n = 3$.

For the rectangular configuration, equation (23) reduces to

$$\begin{aligned}\frac{I_e}{I_{Cs^+}} &= 0.3(n - 1)f \\ &= 0.3\ f \quad \text{for} \quad n = 2 \\ &= 0.6\ f \quad \text{for} \quad n = 3\end{aligned} \tag{26}$$

For values of f from 0.01 to 0.10, this yields possible values of I_e/I_{Cs^+} of 0.003 to 0.030, and 0.006 to 0.060 for $n = 2$ and 3, respectively.

The assumption has been made in this analysis that the only neutral cesium arriving at the accelerator electrode is that emitted uniformly and diffusely from the emitter. It seems reasonable to expect that those atoms that can reach

the accelerator directly (distributed arrival rate) will contribute the minimum amount that can enter into adsorption equilibrium with the accelerator surface. Since electron-emission rates increase with increasing arrival rates, electron-emission rates calculated for this case can reasonably be considered as lower limits for the accelerator temperatures indicated.

On the other hand, if it is assumed that cesium gas fills the interelectrode space, the equilibrium pressure is such that the rate of escape of cesium through the accelerator opening equals the arrival rate into the interelectrode space. This condition yields a maximum arrival rate of cesium at the accelerator electrode, and, hence, electron-emission rates calculated for this case can reasonably be considered as the upper limit.

The calculated values of I_e/I_{Cs^+} (determined over the range of accelerator temperature of interest) are summarized in table I. For the distributed arrival rate, the values given for $f = 0.01$ are associated with the minimum peak values, and those given for $f = 0.10$ are associated with the maximum peak values (figs. 7 and 12).

There was little difference in the total electron-emission rates between the axisymmetric and the rectangular configurations for the condition of distributed arrival rate. The slightly higher local electron-emission rates that resulted for the rectangular configuration were compensated by a lower ratio of accelerator-electrode to ion-emitter area.

For the assumed case of a uniform arrival rate at the electrodes, however, the possible electron-emission currents for the rectangular configuration were considerably lower than for the axisymmetric configuration. This resulted because the value of k was larger for the rectangular configuration (more cesium went directly out the accelerator opening) and because the rectangular configuration had a lower ratio of total electrode area to ion-emitter area.

It is apparent from an examination of table I that electron-emission currents must be considered in interpreting accelerator-electrode-current measurements.

Accelerator-Electrode Materials

All the previous calculations were made by assuming that the accelerator-electrode material was tungsten. Of course, if the electrode were of a different material, the electron-emission characteristics might be different. Currently in use in experimental thrustor designs are materials such as molybdenum, tantalum, copper, stainless steel, and others. From figures 3(b) and (c), it can be seen that the maximum electron emission for a given arrival rate of cesium is lower for molybdenum by a factor of 0.5 to 0.1. This would mean that the maximum emission from a molybdenum electrode would be lower by these factors. Consistent data for electron emission from cesium-coated materials, other than molybdenum or tungsten, in the range of interest here are not available. From the data of reference 11 (with the assumption that the ratios hold at much lower values of cesium arrival rates), it could be concluded that peak emission from tantalum

would be lower than from tungsten by about a factor of 0.5. Reference 11 also indicates that molybdenum would be closer to tungsten than inferred from figures 3(b) and (c). In reference 12, peak electron-emission currents from tantalum are indicated to be greater than from tungsten.

A final noteworthy point is that cesium on oxidized tungsten yields higher peak electron-emission currents than obtained from cesium on nonoxidized tungsten. Oxides of the other metals may have similarly increased electron-emission currents.

In general, then, the variations of electron emission with different electrode materials cannot be stated unequivocally at the present time.

Other Considerations

It might be of interest to know how the use of multiple units, arrayed together to make a large thrustor, would affect the results of this analysis. When units are assembled side by side, the avenues for escape of neutral cesium from the system become restricted to the opening in the accelerator electrode. It seems reasonable to expect that the background gas pressure would tend to approach the assumed uniform distribution.

When the units are side by side, then, the possible electron-emission currents can be relatively high, if the electrode temperature is in the proper range. The monitoring of the electrode temperature, then, would be of considerable importance. In actual thrustor operation, maintaining the accelerator at a temperature about $\pm 100^{\circ}$ K away from that at which peak electron emission occurs can reduce the electron emission by about an order of magnitude (figs. 7 and 12). Anomalous as it may seem at first thought, it may be easier in an actual thrustor to raise the accelerator-electrode temperature (e.g., by improving heat shielding downstream of the accelerator electrode) to prevent high thermionic electron-emission currents.

CONCLUSIONS

The magnitude of thermionic electron emission from ion-thrustor electrodes due to coating by the neutral-cesium propellant was estimated for two configurations by calculating the distributed and peak neutral-atom arrival rates at the electrodes. From assumed electrode temperatures and available literature on the variation of electron emission with arrival rate, local and total electron-emission rates were calculated. The following conclusions were reached:

1. The behavior of the axisymmetric and rectangular configurations was substantially the same.

2. Adsorption conditions, resulting from direct impingement of neutral-cesium atoms from an ionizer, are such that an electron-emission current from an accelerator electrode can be as high as 4 percent of the ion-beam current, if the electrode temperature is near the value yielding maximum electron emission.

3. If neutral cesium does not condense out of the system, and if it can escape only through the opening in the accelerator electrode, a background cesium pressure can build up in the interelectrode space. The electron-emission current from the electrode could then reach a value as high as 40 percent of the ion-beam current, if the accelerator temperature is near that for maximum emission.

4. Electron-emission currents can be reduced by an order of magnitude from the peak values by operating the accelerator at a temperature $\pm 100^{\circ}$ K away from the peak emission temperature.

Lewis Research Center
National Aeronautics and Space Administration
Cleveland, Ohio, May 20, 1963

APPENDIX - SYMBOLS

A	area
f	ratio of neutral-cesium-flow rate to ion-flow rate leaving emitter
I_{Cs^+}	total ion current
I_e	total electron current emitted from accelerator electrode
I_n	total neutral-atom current equivalent
j	ion-current density, amp/m^2
k	fraction of neutral flux passing directly through accelerator opening
L	distance from emitter to accelerator plane
l	distance from point on emitter to point on accelerator plane
n	accelerator width factor, ratio of outer to inner radius of axisymmetric configuration, equal to U/W for rectangular configuration
R	radius of emitter
r	radius variable
U	overall width of accelerator electrode
u	lateral dimension in accelerator plane
V	overall length of accelerator electrode
v	longitudinal dimension in accelerator plane
W	width of rectangular emitter
x	lateral dimension in emitter plane
Y	overall length of rectangular emitter
y	longitudinal dimension in emitter plane
α	angle variable between l and normal
θ	angle variable in emitter or accelerator plane
μ	arrival rate at accelerator
ν_a	neutral-cesium-emission rate from ionizer

ν_{Cs^+} cesium-ion-emission rate from ionizer

ν_e electron-emission rate

Subscripts:

ao accelerator opening

e emitter

r radius variable

u lateral dimension in accelerator plane

v longitudinal dimension in accelerator plane

θ angle variable in emitter or accelerator plane

1 emitter plane

2 accelerator plane

REFERENCES

1. Brewer, G. R., Currie, M. R., and Knechtli, R. C.: Ionic and Plasma Propulsion for Space Vehicles. Proc. IRE, vol. 49, no. 12, Dec. 1961, pp. 1789-1821.

2. Naiditch, Sam, et al.: Ion Propulsion Systems: Experimental Studies. Paper 928-59, Am. Rocket Soc., Inc., 1959.

3. Kerslake, William R.: Charge-Exchange Effects on the Accelerator Impingement of an Electron-Bombardment Ion Rocket. NASA TN D-1657, 1963.

4. Hottel, H. C.: Radiant Heat Transmission. Mech. Eng., vol. 52, no. 7, July 1930, pp. 699-704.

5. Lozgachev, V. I.: Distribution of Molecular Flow on a Surface During Evaporation in Vacuum. Soviet Phys.-Tech. Phys., vol. 7, no. 8, Feb. 1963, pp. 736-744.

6. Mickelsen, William R.: Theoretical Performance of Electrostatic Thrustors with Analytic Space-Charge Flows. NASA TR R-174, 1963.

7. Taylor, John Bradshaw, and Langmuir, Irving: The Evaporation of Atoms, Ions, and Electrons from Caesium Films on Tungsten. Phys. Rev., vol. 44, no. 6, Sept. 15, 1933, pp. 423-458.

8. Aamodt, R. L., Brown, L. J., and Nichols, B. D.: Thermionic Emission from Molybdenum in Vapors of Cesium and Cesium Fluoride. Jour. Appl. Phys., vol. 33, no. 6, June 1962, pp. 2080-2085.

9. Husmann, O. K.: Experimental Evaluation of Porous Materials for Surface Ionization of Cesium and Potassium. Preprint 2359-62, Am. Rocket Soc., Inc., 1962.

10. Work, G. A.: Development of an Ion Rocket Engine System for Attitude Control and Station Keeping. Quarterly Prog. Rep. 1, Hughes Res. Labs., Jan. 28, 1963.

11. Houston, John M.: Thermionic Emission of Refractory Metals in Cesium Vapor. Proc. Round Table Discussion on Cathode Emission Investigation and Experimental Techniques for Fabricating and Operating Thermionic Cells. June 1-2, 1961. Appendix F-1, PIC-ELE-TI 3/3, Power Info. Center, Univ. Penn., June 30, 1961.

12. Webster, H. F.: Thermionic Emission from a Tantalum Crystal in Cesium or Rubidium Vapor. Jour. Appl. Phys., vol. 32, no. 9, Sept. 1961, pp. 1802-1803.

TABLE I. - PEAK VALUES OF RATIO OF ELECTRON-EMISSION TO ION-EMISSION CURRENT

Accelerator size, n	Distributed arrival rate		Uniform arrival rate	
	Fraction of neutral cesium leaving emitter, f			
	0.01	0.10	0.01	0.10
	Ratio of electron-emission to ion-emission current, I_e/I_{Cs^+}			
Axisymmetric configuration				
2	0.0018	0.024	0.015	0.15
3	.0029	.042	.040	.40
Rectangular configuration				
2	0.0013	0.014	0.003	0.03
3	.0019	.024	.006	.06

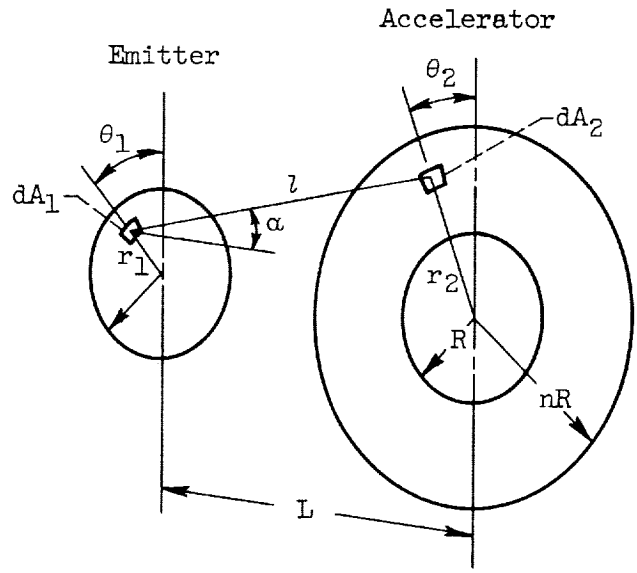

Figure 1. - Schematic illustration of axisymmetric configuration.

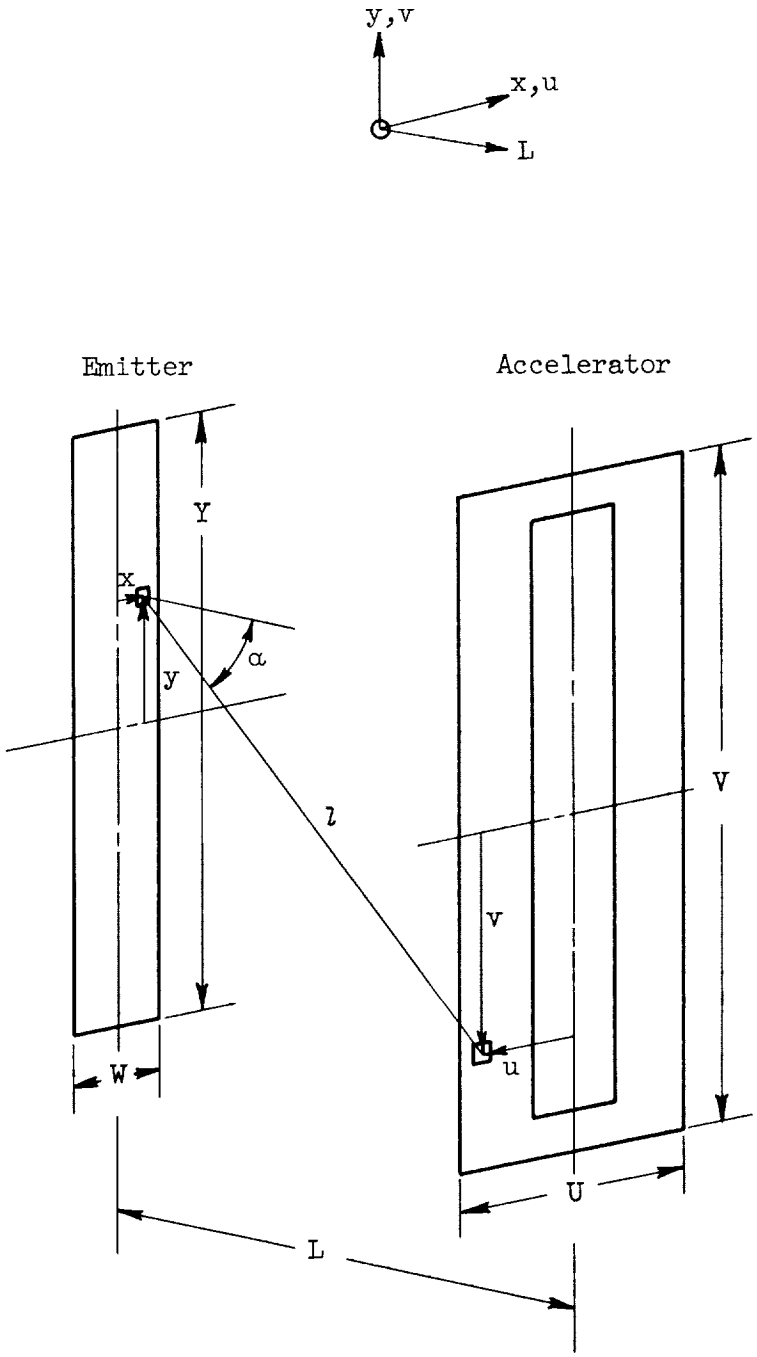

Figure 2. - Schematic illustration of rectangular-beam configuration.

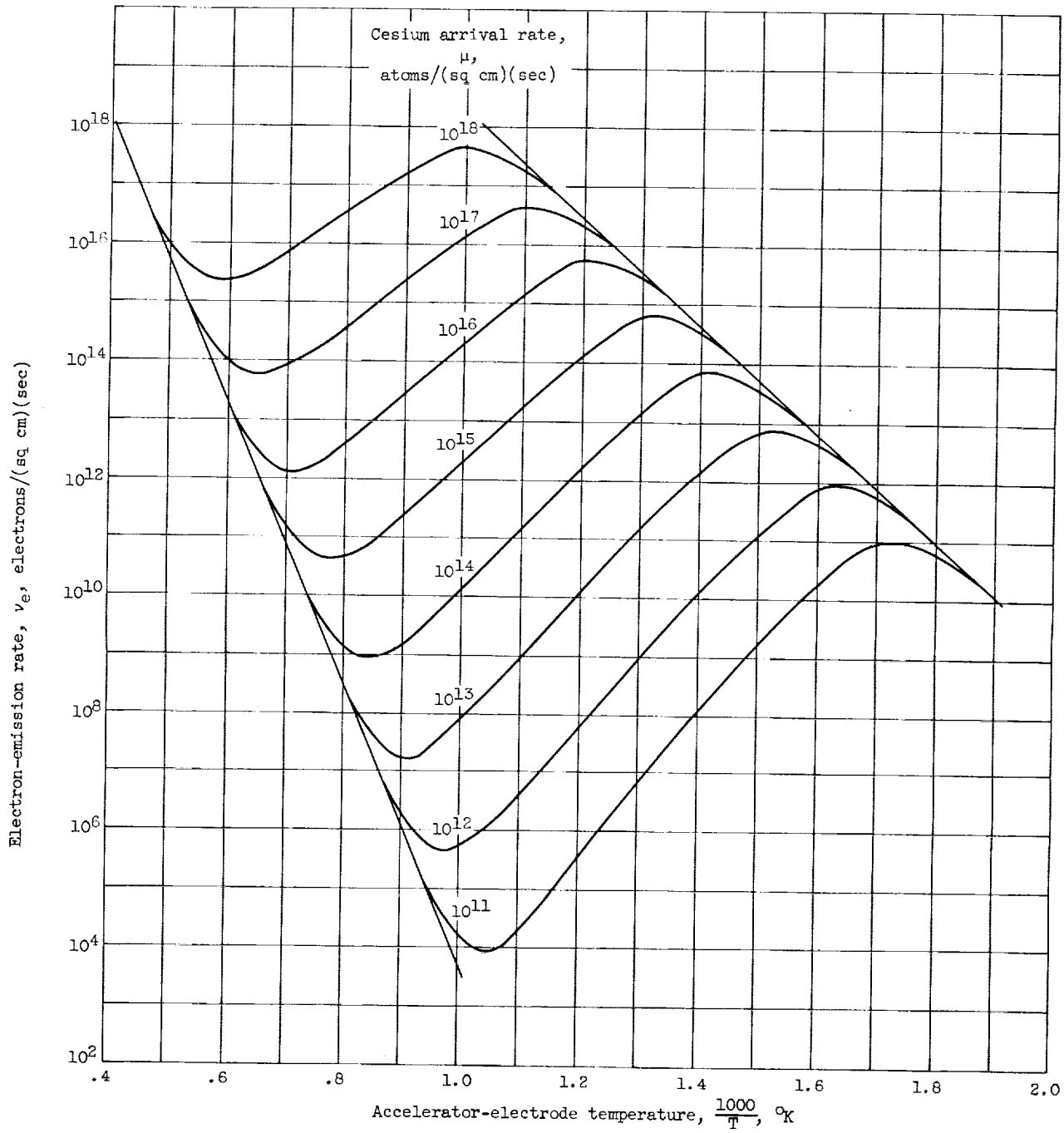

(a) As function of accelerator-electrode temperature for tungsten.

Figure 3. - Electron emission from refractory metal in cesium atmosphere.

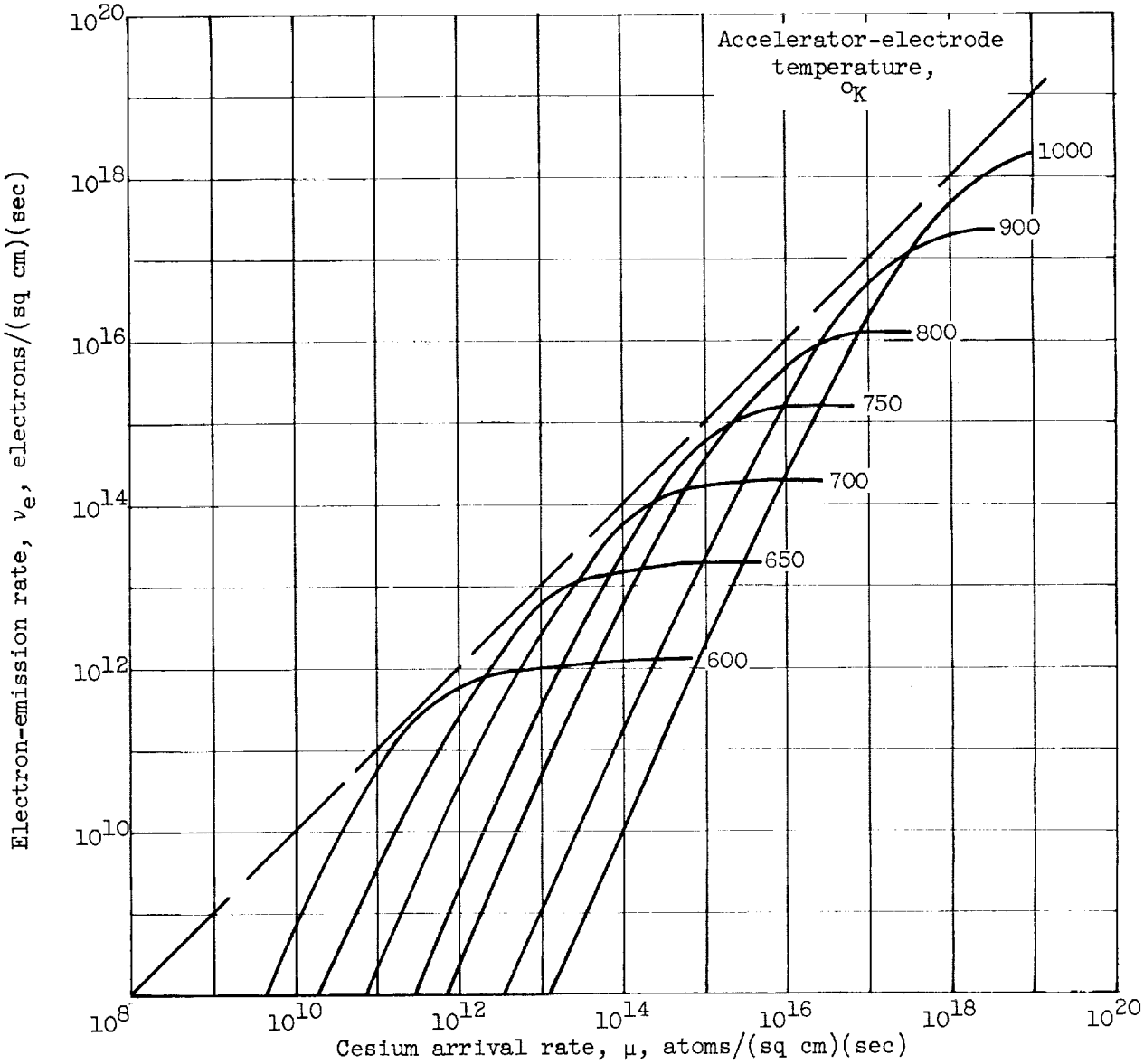

(b) As function of cesium arrival rate for tungsten.

Figure 3. - Continued. Electron emission from refractory metal in cesium atmosphere.

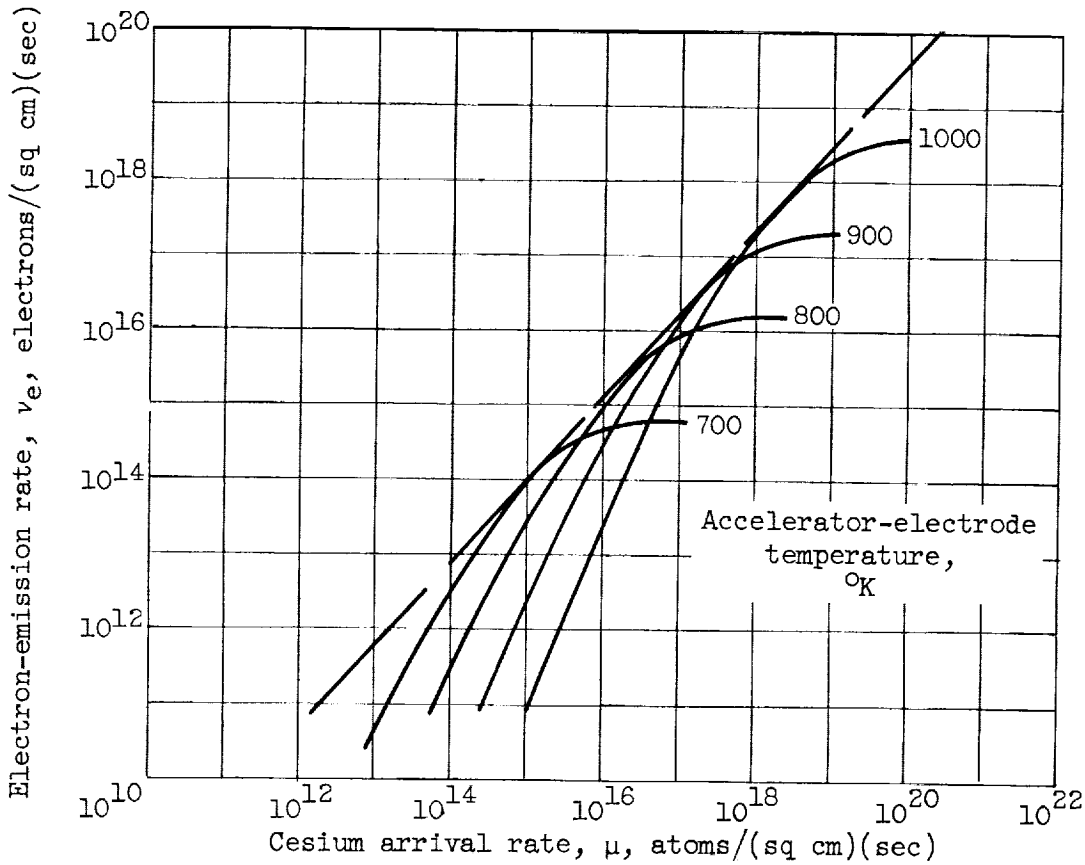

(c) As function of cesium arrival rate for molybdenum.

Figure 3. - Concluded. Electron emission from refractory metal in cesium atmosphere.

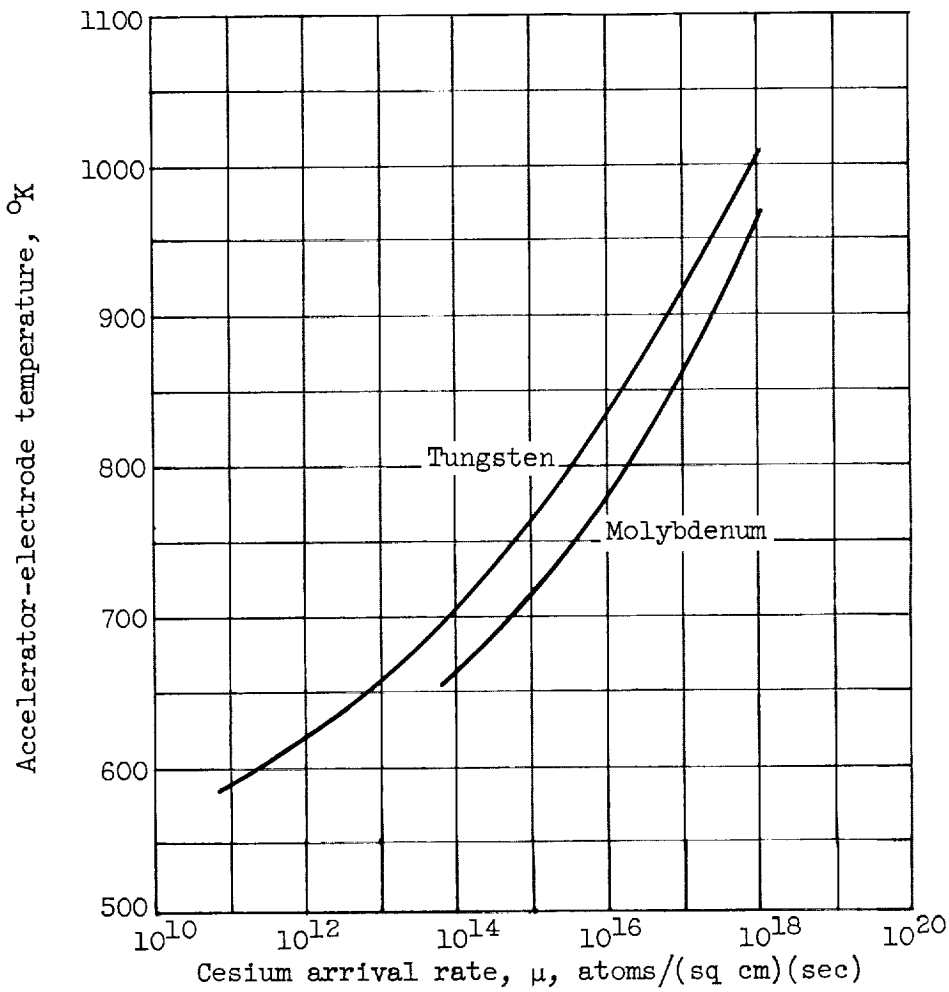

Figure 4. - Temperature at which peak electron emission occurs for given arrival rate of cesium on tungsten and molybdenum.

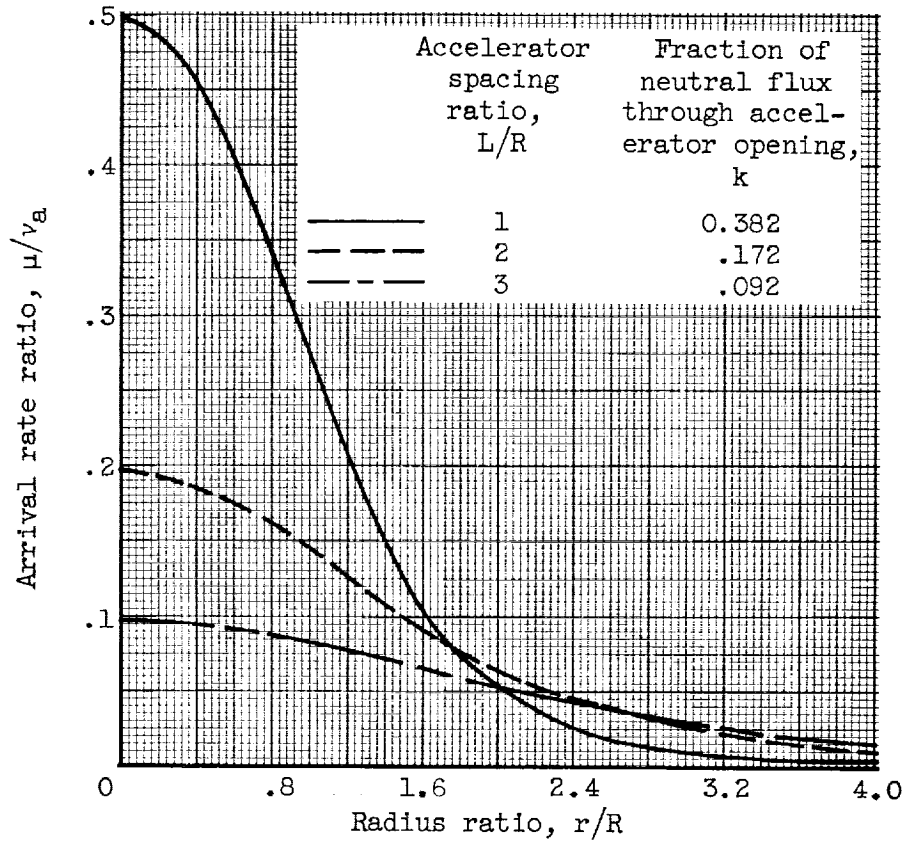

Figure 5. - Variation of arrival-rate ratio with radius ratio and accelerator spacing ratio for axisymmetric configuration.

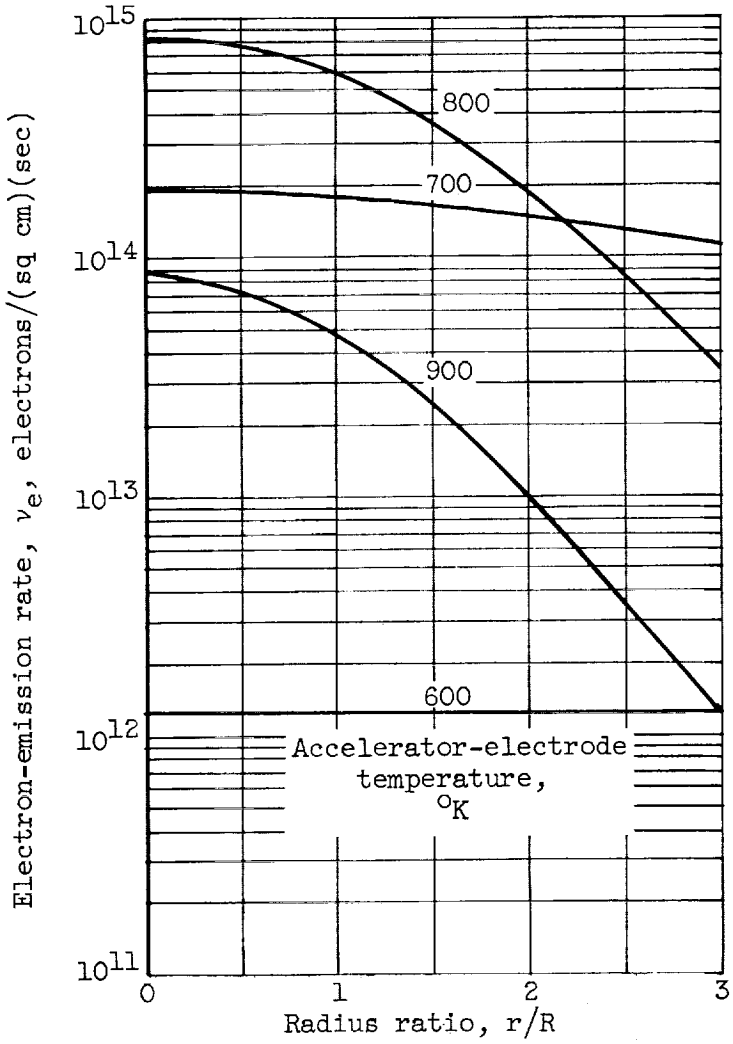

Figure 6. - Distribution of electron-emission rate with radius ratio at accelerator plane for axisymmetric configuration. Accelerator spacing ratio, 2; neutral-cesium-emission rate, 10^{16} atoms per square centimeter per second; tungsten electrode.

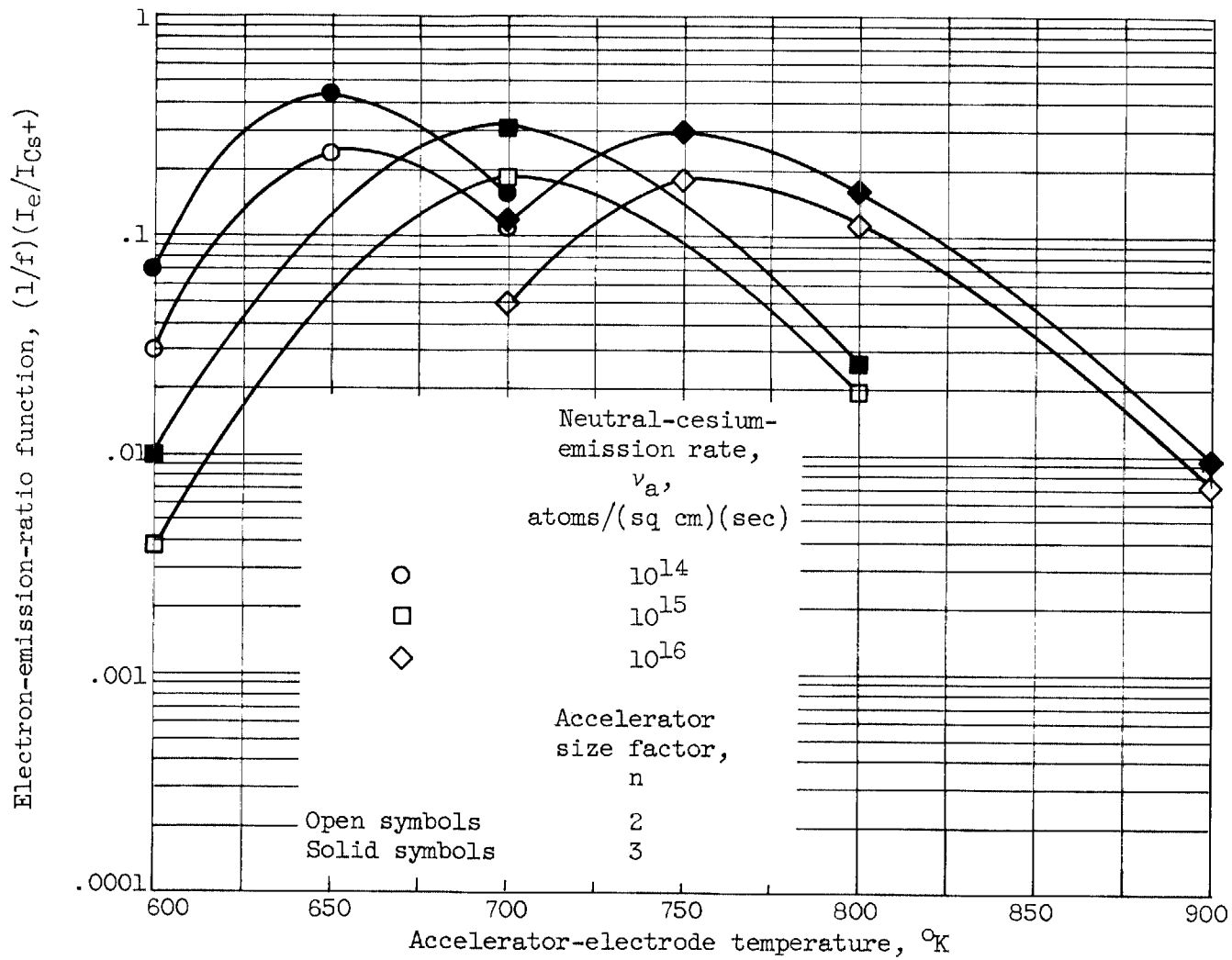

Figure 7. - Ratio of total electron to total ion emission as function of accelerator temperature for axisymmetric configuration. Accelerator spacing ratio, 2; tungsten electrode; distributed arrival rate.

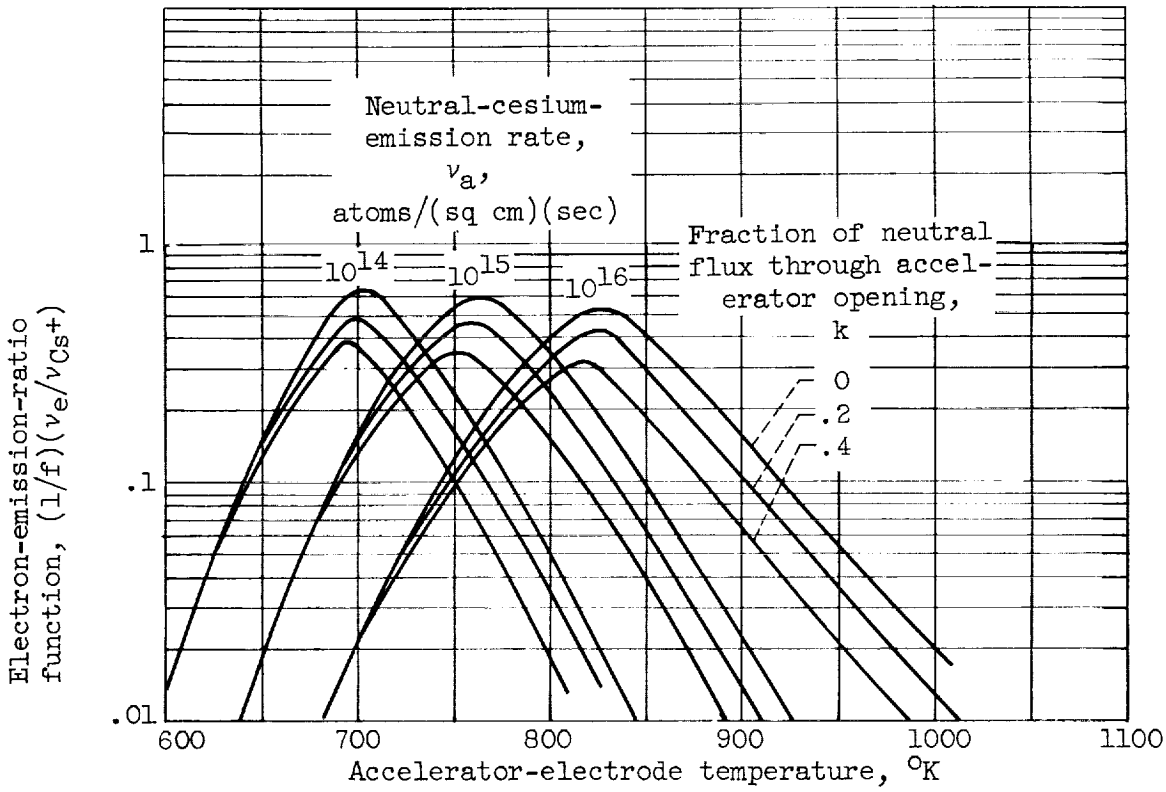

Figure 8. - Ratio of total electron to total ion emission as function of electrode temperature for either axisymmetric or rectangular configuration. Tungsten electrode; uniform arrival rate.

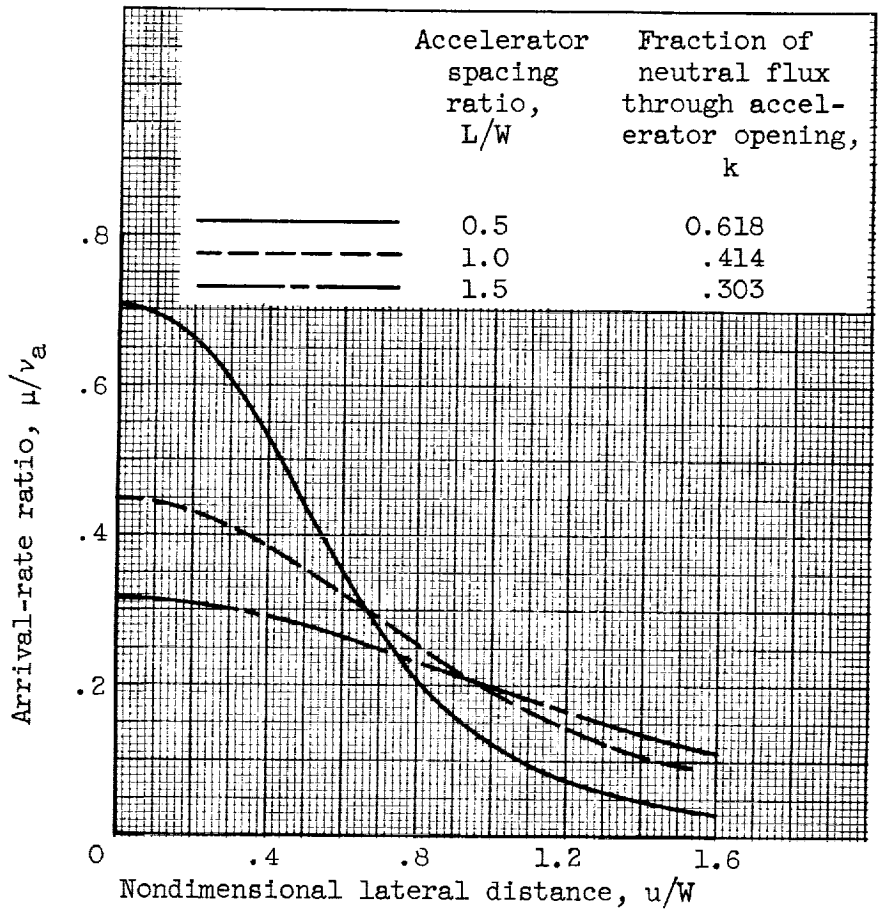

Figure 9. - Variation of arrival-rate ratio in u-direction with various accelerator spacing ratios for rectangular configuration. Infinite-length emitter; distributed arrival rate.

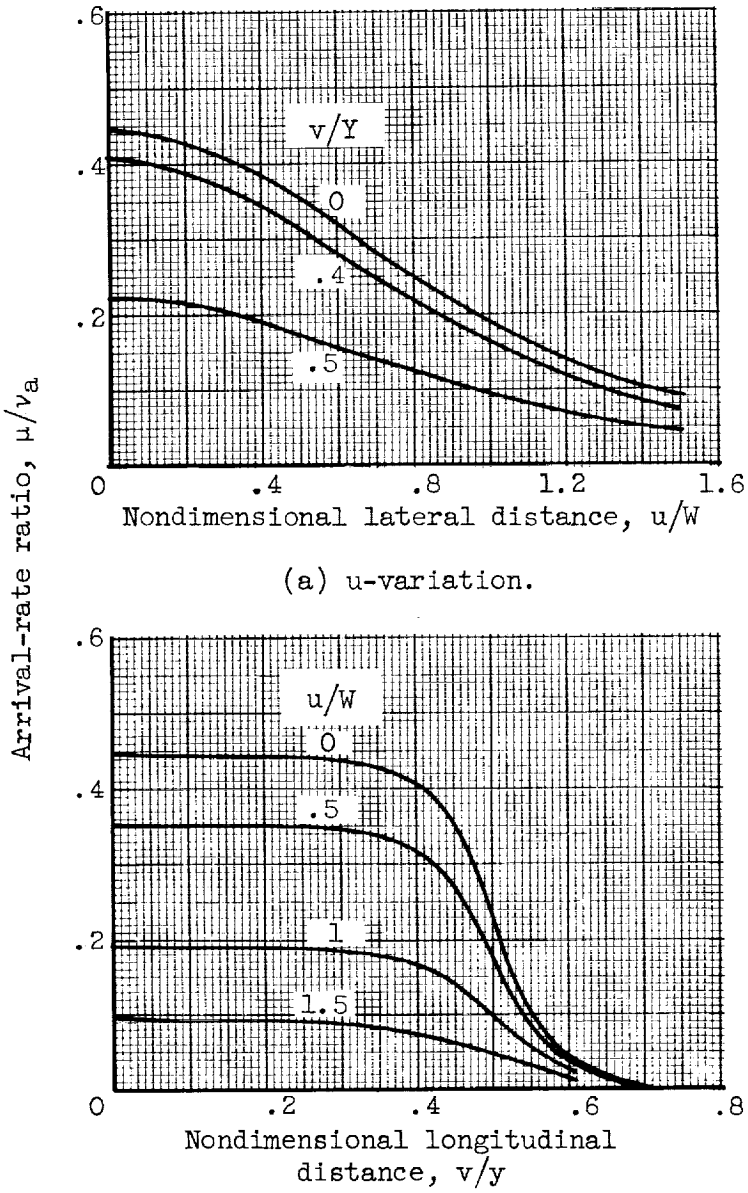

(a) u-variation.

(b) v-variation.

Figure 10. - Variation of arrival-rate ratio in u- and v-directions for rectangular configuration. Nondimensional emitter length, 10; nondimensional distance from emitter to accelerator, 1.

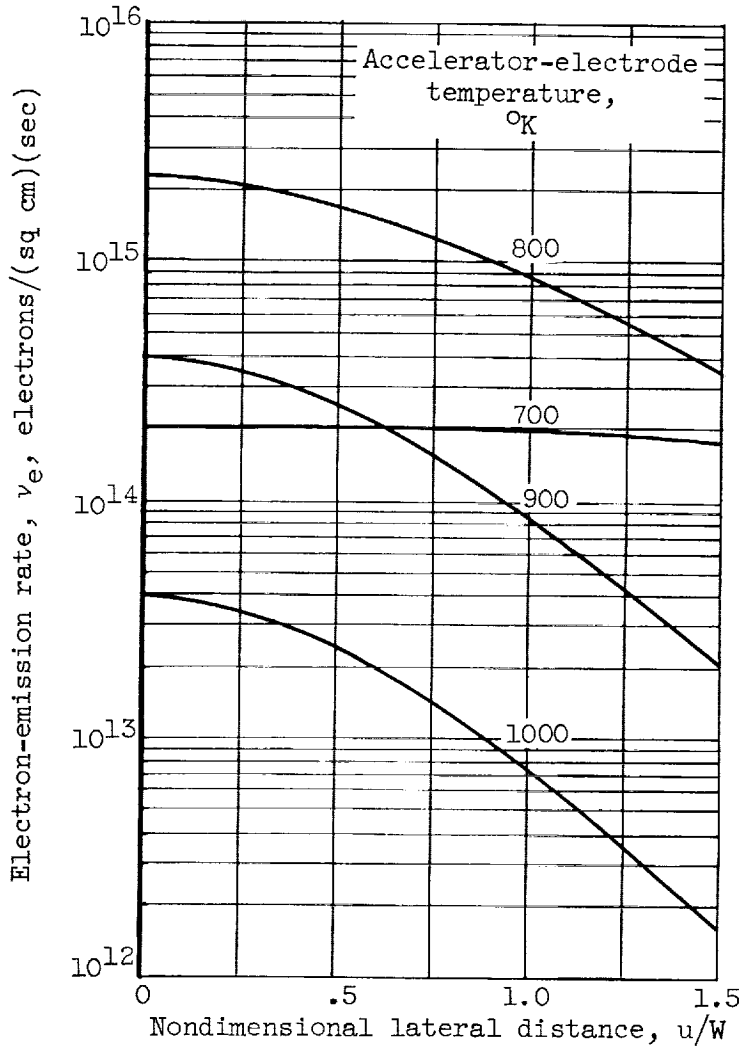

Figure 11. - Distribution of electron-emission rate in u-direction at accelerator plane for rectangular configuration. Infinite-length emitter; nondimensional distance from emitter to accelerator, 1; neutral-cesium-emission rate, 10^{16} atoms per square centimeter per second; tungsten electrode.

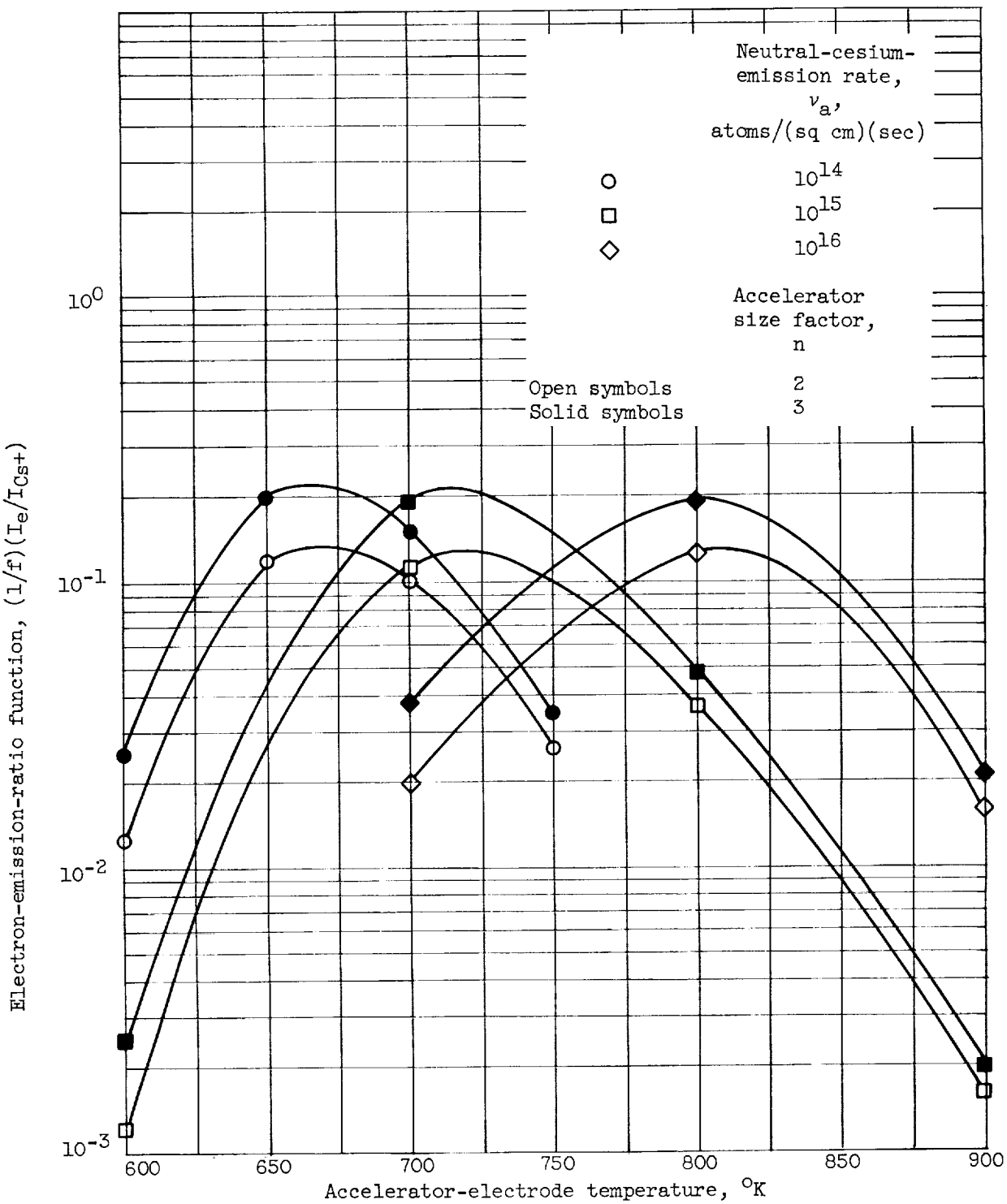

Figure 12. - Ratio of total electron to total ion emission as function of electrode temperature for rectangular configuration. Infinite-length emitter; nondimensional distance from emitter to accelerator, 1; tungsten electrode; distributed arrival rate.